Weak localization in $1T$-$TiSe_2$ microflakes

Zhaoguo Li,* Jicheng Zhang, Minjie Zhou, Yong Zeng, Daojian Qi, and Jia Li
Research Center of Laser Fusion, China Academy of Engineering Physics, Mianyang 621900, China

(Received 17 January 2020; revised manuscript received 2 March 2020; accepted 19 March 2020; published 10 April 2020)

We have studied the electrical transport in the charge-density wave material $1T$-$TiSe_2$ microflakes. In the low temperatures, the logarithmic temperature-dependent resistivity corrections were observed. In particular, the negative magnetoresistances in low magnetic fields were further measured and well described by the Hikami-Larkin-Nagaoka theory. All the experimental results demonstrate the weak localization effect in the $1T$-$TiSe_2$ microflakes. Furthermore, the power-law dependence of the extracted phase coherence length on temperature is $\sim T^{-0.6}$, indicating the presence of the two-dimensional electron-electron interaction in the $1T$-$TiSe_2$ microflakes.

DOI: 10.1103/PhysRevB.101.155111

I. INTRODUCTION

Recently, the layered transition-metal dichalcogenides have aroused much research interest due to their novel quantum or topological properties and the extensive applications. $1T$-$TiSe_2$ is an octahedral structure crystal, which undergoes a semimetal to charge-density wave (CDW) phase transition at around 200 K [1]. The CDW state was first pointed out by Peierls, who found that a one-dimensional metal coupled to the underlying lattice is not stable at low temperatures [2,3]. One result of the Peierls instability is the development of a spatially periodic distortion of the crystal lattice. This periodic structural distortion of the arrangement of ions in the metal is accompanied by a corresponding spatial modulation of the charge density, and further leads to a gap at the Fermi energy. The CDW transition in $1T$-$TiSe_2$ is of second order, forming a commensurate $2\times2\times2$ superlattice structure below the CDW transition temperature ($T_{CDW} \approx 200$ K) [1,4]. The origin of the CDW transition in $1T$-$TiSe_2$ remains in debate so far. The candidate mechanisms include the excitonic insulator [5] and the Jahn-Teller effect [6]. Furthermore, the superconductivity of the $1T$-$TiSe_2$ was also observed by Cu or Pd intercalation [7,8] and applying pressure [9] or electrostatic gating [10]. These results underscore the complex electrical transport properties in $1T$-$TiSe_2$.

The lattice distortion in CDW materials will lead to a gap opening at the Fermi energy while $T < T_{CDW}$. We can expect to observe a metal-insulator transition near T_{CDW}, as experimentally confirmed in the blue bronzes [11]. However, in some CDW materials, such as $NbSe_3$ [12], the $\rho(T)$ curve at $T < T_{CDW}$ keeps the metallic behavior. One of the interpretations suggests that the CDW is formed (gap opened) in one metallic chain, and the electronic structure in another inequivalent metallic chain remains in a normal metal state. Therefore, only a portion of the Fermi surface is gapped, and the metallic transport behavior survives below T_{CDW}. An interesting feature is that the partially gapped Fermi surface provides the confinement electronic states in the momentum space. We expect to observe the quantum interference effect in such confinement systems. Cao *et al.* [13] first observed the weak localization (WL) transport features in the CDW VSe_2 nanosheets. Recently, Moya *et al.* [14] reported the WL effect in the polycrystalline $TiSe_2$ samples. However, the experimental evidence of the WL transport in the single-crystalline $TiSe_2$ flakes remains absent.

In this work, we report the magnetotransport properties of the CDW material $1T$-$TiSe_2$ microflakes. The CDW transition temperature was extracted at 185 K by analyzing the temperature dependence of resistivity. The Hall-effect measurement revealed the carrier-type changes from p type at high temperatures to n type in low temperatures, corresponding to critical temperature at ~205 K. For the magnetoresistance (MR) curves at low temperatures ($T \lesssim 13$ K), the high-field MR presents a B^2 law which corresponds to the classical Boltzmann transport. In low fields, a MR peak was clearly observed; it is the result of the WL effect. The extracted phase coherence length satisfies the scaling law of $L_\phi \propto T^{-0.6}$, which implies that the electron-electron interaction dominates the dephasing mechanism in $1T$-$TiSe_2$.

II. EXPERIMENT

The $TiSe_2$ single crystals were grown by chemical vapor transport with the transport agent iodine. High-purity titanium and selenium powers were mixed with a Ti:Se atomic ratio of 1:2.05. The mixture and 5 mg/cm^3 of iodine were sealed in evacuated quartz tubes. The tubes were placed into a two-zone tube furnace. The powder zone was heated to 670 °C and the $TiSe_2$ crystals were synthesized at 600 °C zone for a period of 2 weeks. The crystal structure of $1T$-$TiSe_2$ was confirmed by x-ray diffraction (XRD) [Fig. 1(a)]. The components of the $1T$-$TiSe_2$ crystals were measured by the energy-dispersive x-ray spectrometry (EDXS). As shown in Fig. 1(b), the EDXS result gave a Ti:Se atomic ratio of 1:2, indicating the stoichiometric ratio of the crystals.

*lizhaoguo@caep.cn

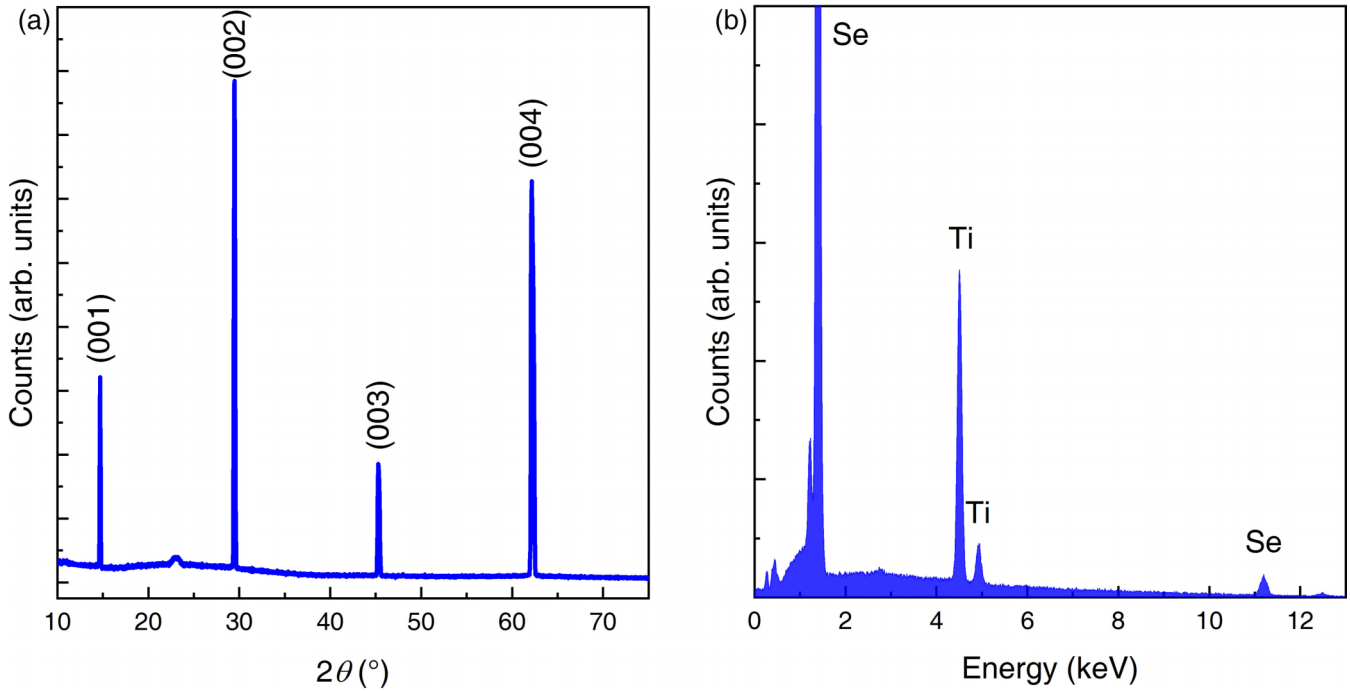

FIG. 1. Structural characterizations of the $1T$-$TiSe_2$ crystals. (a) The x-ray-diffraction pattern of the $1T$-$TiSe_2$ crystals. The strong $(00n)$ peaks indicate the nice crystalline of the bulk crystals. (b) The energy-dispersive x-ray spectrum of the $1T$-$TiSe_2$ crystals, which indicates the stoichiometric ratio of the crystals.

The thin $1T$-$TiSe_2$ microflakes were mechanically exfoliated from the single crystals onto the 300-nm SiO_2/Si substrates. The Ti (10 nm)/Au (100 nm) electrodes were well patterned onto the microflakes by standard photolithography followed by an electron-beam evaporation deposition and lift-off process. The geometric sizes of the microflakes were determined by the atomic force microscopy. The temperature dependence of resistance and MR measurements were carried out on a Quantum Design Physical Property Measurement System. Herein, we totally measured two devices, S1 and S2. Their parameters are summarized in Table I. S1 is a six-probe Hall device; both resistance and Hall effect were measured. In all cases, the magnetic-field B was applied perpendicular to the sample plane.

III. RESULTS AND DISCUSSION

A. Temperature dependence of resistivity

Figure 2(a) shows the temperature dependence of the resistivity (ρ) in the $1T$-$TiSe_2$ microflakes. Both curves present a peak near $T_P \approx 165$ K. The resistivity increased with decreasing temperature at $T > T_P$, indicating a "insulator" transport behavior. While $T < T_P$, the metallic transport behavior is observed, that is, the resistivity decreased with decreasing temperature. As we know, the $1T$-$TiSe_2$ crystal is a semimetal at room temperature. Therefore, a metallic transport behavior should be observed near room temperature. It seems to contradict the experimental results. In order to understand this paradox, we first determine the CDW transition temperature of the $1T$-$TiSe_2$ microflakes.

TABLE I. Parameters of the $1T$-$TiSe_2$ devices. L is the center-to-center distance between the two electrodes along the current direction. W and t are the width and thickness of the microflakes, respectively. ρ is the electrical resistivity at $T = 2$ K.

Sample	L (μm)	W (μm)	t (nm)	ρ ($\mu\Omega$ m)
S1	20	19	77	1.75
S2	10	6	45	4.04

To accurately determine the CDW phase-transition temperature (T_{CDW}) of the $1T$-$TiSe_2$ microflakes, the derivative of the resistivity with the temperature ($d\rho/dT$) was calculated, as shown in Fig. 2(b). The minimum values of the $d\rho/dT$ indicate the T_{CDW} is $\approx$185 K, which is in agreement with the reported values [1,4,7,9,10]. Therefore, the observed insulator transport behavior in the mediated temperature range (near T_{CDW}) resulted from the competition between the insulator and metal states. Actually, the metallic transport behavior can be observed in the higher temperatures [1].

Moreover, the "metal" $\rho(T)$ behavior is observed while $T < T_P$ in our $1T$-$TiSe_2$ microflakes [Fig. 2(a)]. This phenomenon seems to conflict with the prediction of the metal-insulator transition in CDW phase transition. Its accurate mechanism remains in debate. One mechanism suggests that the Fermi surface was partially gapped while the CDW transition was occurring [1]. Another mechanism claims that the resistivity peak in $1T$-$TiSe_2$ corresponds to the crossover between a low-temperature regime with electronlike carriers only to a high-temperature regime with the thermally activated holelike carriers [15]. The latter mechanism does not need the CDW transition at all. Nevertheless, the more experimental

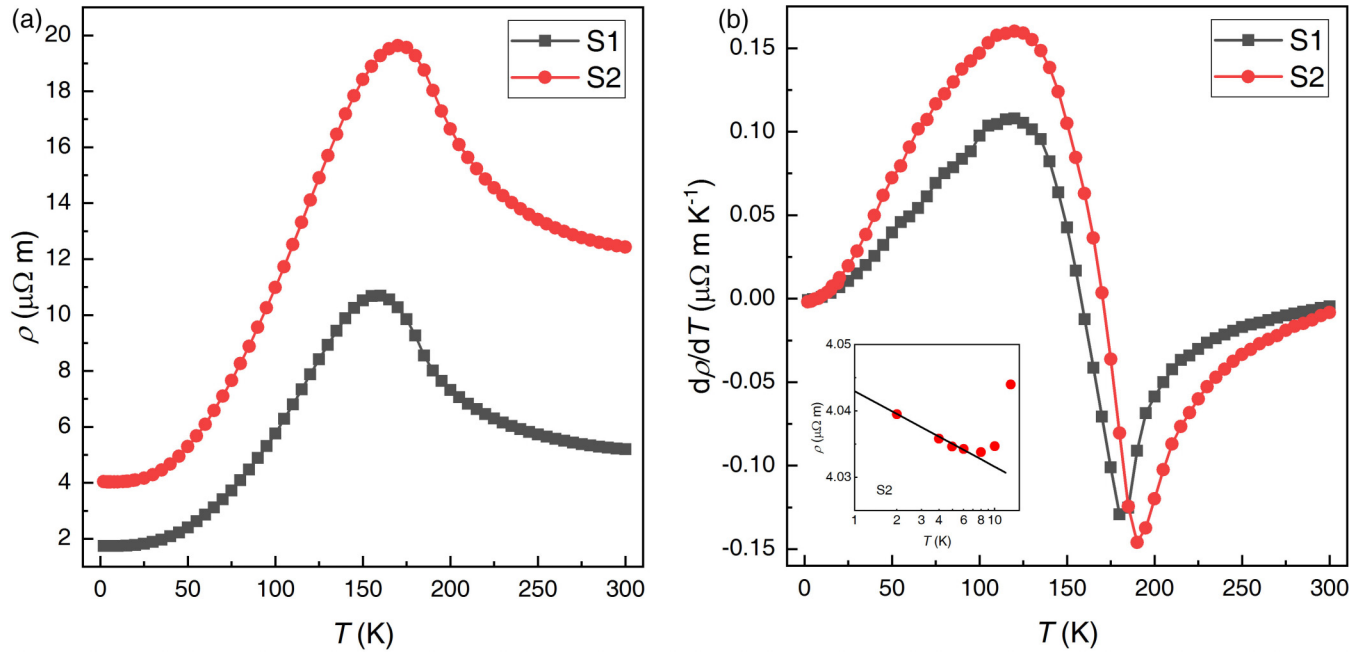

FIG. 2. Charge-density wave transition in the $1T$-$TiSe_2$ microflakes. (a) The temperature dependence of the measured resistivity ρ. (b) The derivative of the resistivity ($d\rho/dT$) plotted as a function of temperature. The minimum values of the $d\rho/dT$ curves indicate the CDW transition temperature (T_{CDW}) is ~185 K. The inset shows the upturn of the ρ-T curve at the low-temperature regime; the solid curve is the best fitting of $\rho \propto \ln T$.

and theoretical work is required to appraise the detailed physical mechanisms.

At the ultralow temperatures ($T \lesssim 8$ K), the resistivity was slightly increased while the temperature decreased [the inset of Fig. 2(b)]. This phenomenon can be well understood by the WL effect. The WL effect described the electronic wave interference phenomenon in a disorder medium [16]. The constructive interference occurred between the forward and the backward directions of propagation, resulting in a backscattering probability enhancement. It leads to an additional contribution to the resistivity superimposed to the classical Boltzmann contribution. According to the WL scaling theory [16], the corrected resistivity for a two-dimensional (2D) system is given by $\rho \propto \ln T$. As shown in the inset of Fig. 2(b), the experimental $\rho(T)$ data meet the prediction of the WL theory. Below, the WL effect in our $1T$-$TiSe_2$ microflakes will be further confirmed by MR analysis.

B. Hall effect

Figure 3(a) displays the Hall resistivity ρ_{xy} vs B curves at various temperatures between 2 ~ 300 K of sample S1. One obvious result is that the carrier type is changed while the temperature is decreasing. The transition temperature can be estimated as $T_R \approx 205$ K; this value is close to that reported previously [1]. Therefore, we can conclude that the hole carriers (p type) dominate the high-temperature ($T > T_R$) transport, and the low-temperature ($T < T_R$) transport properties are dominated by the electron carriers (n type). The carrier concentration and mobility are also extracted, as shown in Fig. 3(b). For example, the electron concentration is $5.0\times10^{19}\,cm^{-3}$ and the electron mobility is $722\,cm^2\,V^{-1}\,s^{-1}$ at 2 K.

Now, we can estimate the transport parameters of the $1T$-$TiSe_2$ microflakes. According to the free-electron model, the Fermi wave vector can be calculated as $k_F = (3\pi^2 n)^{1/3} = 1.14\times10^9$ m^{-1} at $T = 2$ K. The Fermi wavelength $\lambda_F = \frac{2\pi}{k_F} = 5.5$ nm is also obtained. Then, we can obtain $\rho\ell = \frac{3\pi^2\hbar}{k_F^2 e^2} = 9.34\times10^{-14}\,\Omega\,m^2$, where $\hbar$ is Planck's constant and e is the electron charge. And, the elastic mean-free path $\ell \approx 53$ nm is further obtained by using the resistivity ρ. Obviously, the electron transport in the $1T$-$TiSe_2$ microflakes is in the classical diffusive regime since $\lambda_F \ll \ell \ll L$, where L is the sample size. By using the effective electron mass $m_e^* = 3.8m_e$ of $1T$-$TiSe_2$ crystals [15], the Fermi velocity $v_F = \frac{\hbar k_F}{m_e^*} = 3.5\times10^4$ m/s is estimated, where m_e is the free-electron mass. The diffusion constant is finally obtained, $D = \frac{1}{3}v_F\ell = 6.2\,cm^2/s$. The small diffusion constant leads to the low mobility in the $1T$-$TiSe_2$ microflakes. As shown in Fig. 1(a), the small XRD peak near 23° may originate from the (100) plane of Se crystals, indicating the existence of the Se microcrystals or clusters in the $1T$-$TiSe_2$ crystals. Moreover, the native defects, such as intercalated Ti atoms, Se vacancies, etc., also act as the scattering centers in the $1T$-$TiSe_2$ crystals [17]. Therefore, both of the native and extrinsic defects limit the carrier mobility of the $1T$-$TiSe_2$ microflakes.

C. Magnetoresistance

Figure 4 presents the magnetotransport properties of the $1T$-$TiSe_2$ microflakes. The high-field ($B \gtrsim 2$ T) MR can be well fitted by a B^2 law, which demonstrates the classical orbit MR effect arising from the Lorentz force. Interestingly, a notable MR peak is observed in the low-field regime ($B \lesssim 2$ T). This is a typical magnetotransport evidence of the WL effect.

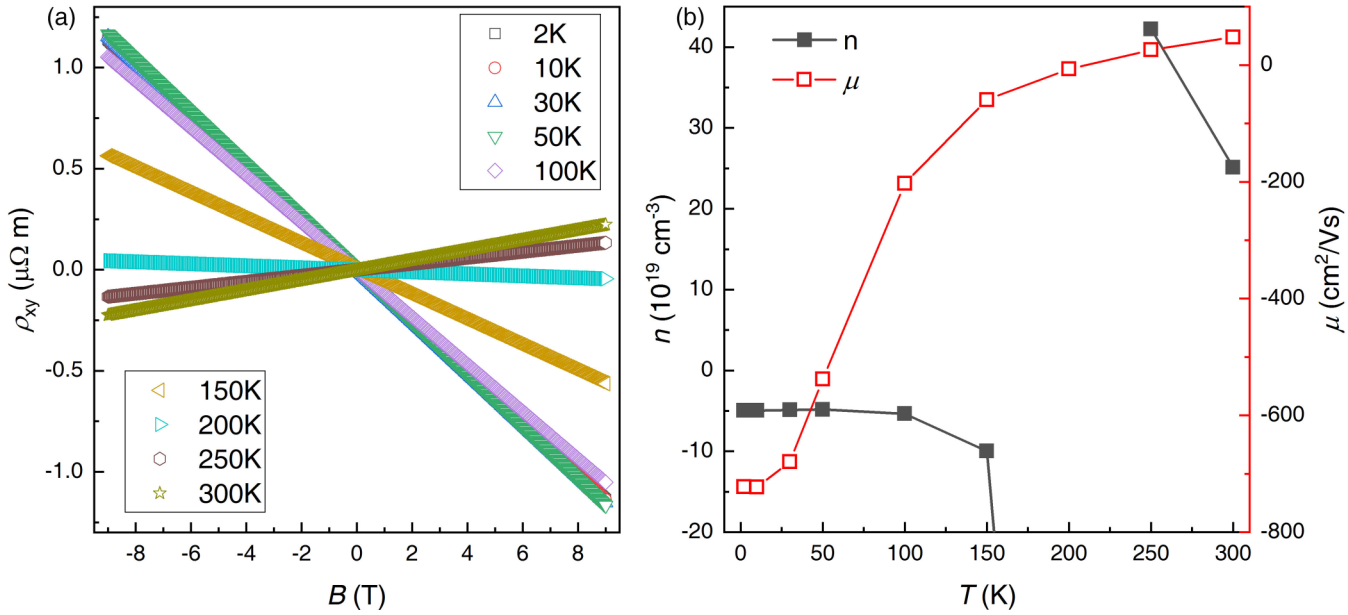

FIG. 3. Hall transport of the 1T-$TiSe_2$ microflakes (sample S1). (a) The Hall resistivity ρ_{xy} plotted as a function of the magnetic field at various temperatures (2–300 K). It is clear that the carrier type changes from p type at high temperatures to n type in low temperatures; the critical temperature is around 205 K. (b) The temperature dependence of the carrier concentration n and the mobility μ.

As discussed above, the WL effect describes the enhancement backscattering probability of the time-reversal paths. This enhancement effect will be suppressed while applying a magnetic field; it leads a decrease of the resistivity. When the magnetic field continues to increase and exceeds a certain threshold value, the quantum coherence of the electrons completely vanishes, and the MR returns to the classical orbit MR. With temperature increasing, the quantum coherence of the carriers will be disturbed by the electron-electron or electron-phonon interactions; we thus observed that the WL effect gradually disappeared. As shown in Fig. 4(b), the MR peak near zero field is almost gone while $T \gtrsim 13$ K.

Quantitatively, the 2D WL magnetoconductance (MC) can be described by the famous Hikami-Larkin-Nagaoka

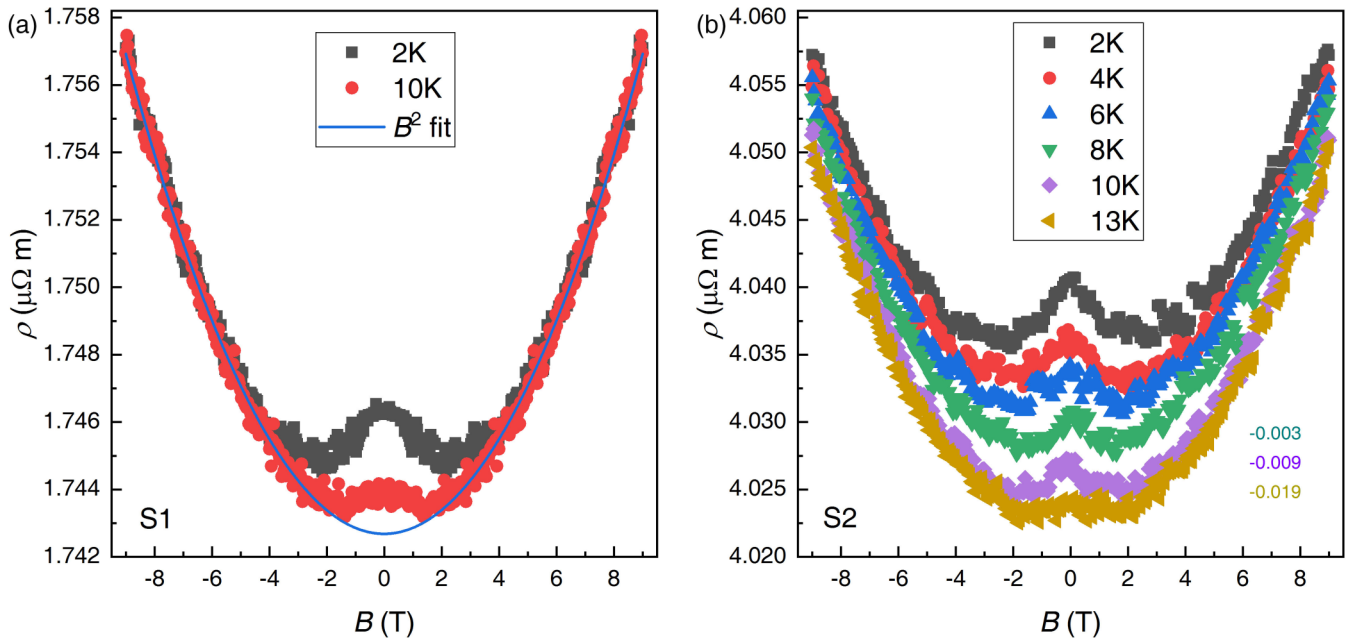

FIG. 4. Magnetoresistance of the 1T-$TiSe_2$ microflakes. (a) The MR curves of sample S1 at 2 and 10 K. The solid curve is the best fitting of $\rho \propto B^2$. (b) The MR curves of sample S2 at several constant temperatures as indicated. For clarity, the MR curves of 8, 10, and 13 K are shifted vertically with −0.003, −0.009, and −0.019 μΩ m respectively. The resistivity peaks near zero fields can be ascribed to the weak localization (WL) effect. At the high fields ($B > 2$ T), the parabolic MR curves are the results of the classical Boltzmann transport.

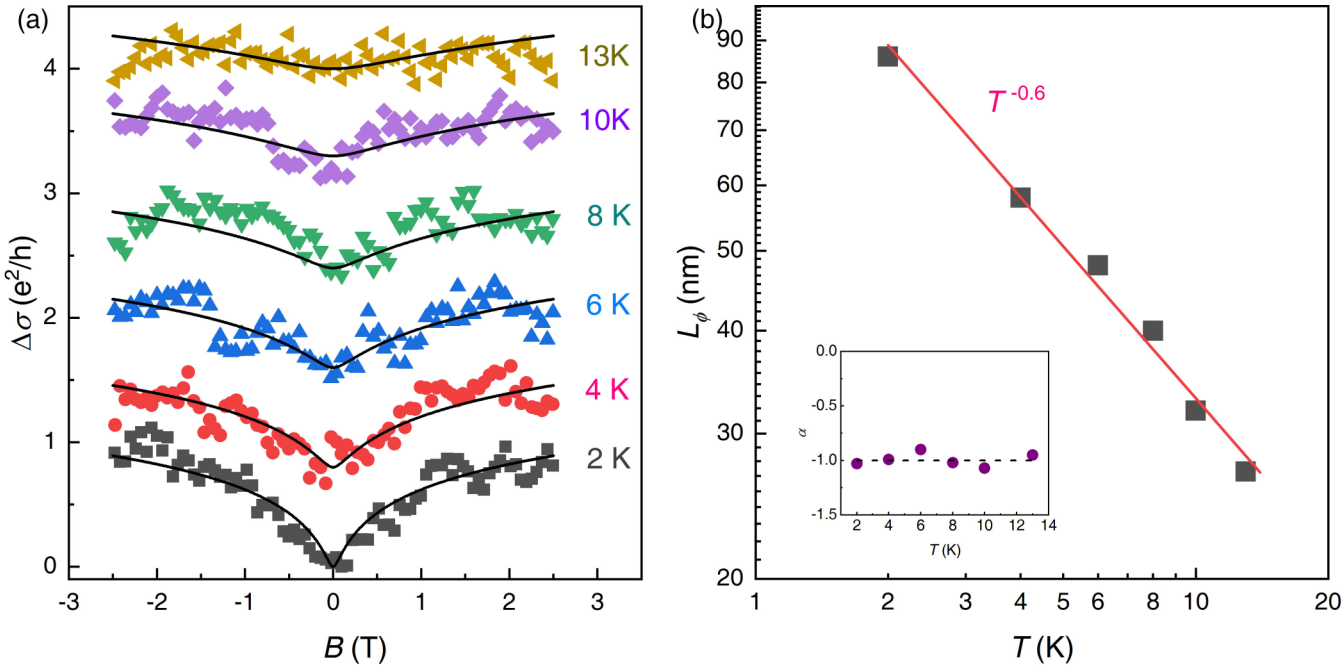

FIG. 5. WL analysis of the low-field MR in the $1T$-$TiSe_2$ microflakes (sample S2). (a) Low-field magnetoconductance for different temperatures, where $\Delta\sigma(B) = \sigma(B) - \sigma(B = 0)$ and $\sigma = L/(WR)$ is the 2D conductivity. The solid curves are the best fits to the Hikami-Larkin-Nagaoka equation. For clarity, each curve is shifted vertically by $0.8\,e^2/h$ with respect to the adjacent curve. (b) The extracted dephasing length L_ϕ plotted as a function of the temperature. The solid curve is the result of the fitting with a power-law function $L_\phi \propto T^{-\beta}$, with $\beta = 0.6$. The inset shows the temperature dependence of the extracted prefactor α, the dashed line indicates $\alpha = -1$ and is a guide to the eye.

formula [18]

$$\Delta\sigma(B) = \frac{\alpha e^2}{2\pi^2\hbar}\left[\ln\left(\frac{\hbar}{4eL_\phi^2 B}\right) - \psi\left(\frac{1}{2} + \frac{\hbar}{4eL_\phi^2 B}\right)\right], \quad (1)$$

where $\Delta\sigma(B) = \sigma(B) - \sigma(B = 0)$ and $\sigma = L/(WR)$ is the 2D conductivity; α is a coefficient indicating the type of localization, $\alpha = -1$ for WL effect corresponding to the weak spin-orbit scattering case, and $\alpha = 1/2$ for weak antilocalization effect corresponding to the strong spin-orbit scattering case; L_ϕ is the phase coherence length and $\psi(x)$ is the digamma function. As shown in Fig. 5(a), we have fitted the low-field MC by using Eq. (1) [the solid curves in Fig. 5(a)]. We can see that the theoretical equation well describes our experimental data. The typical fitting parameters are $\alpha = -1.03$ and $L_\phi = 86$ nm at $T = 2$ K. It is revealed that L_ϕ is larger than the sample thickness ($t = 45$ nm for S2). Therefore, the MC data analysis described above is reasonable by using the 2D WL theory. Furthermore, the value of L_ϕ is comparable with that of the electron elastic mean-free path, that is, $\lambda_F \ll \ell \sim L_\phi \ll L$. It specifies that the classical diffusive transport plays a dominant role in the $1T$-$TiSe_2$ microflakes, and the WL corrections should vanish quickly with increasing of the field and temperature.

The temperature dependence of the extracted α is shown in the inset of Fig. 5(b). As can be seen, the α values are insensitive to the temperature and close to the theoretical value ($\alpha = -1$). It demonstrates the WL origin of the low-field negative MR in our $1T$-$TiSe_2$ microflakes. The phase coherence length L_ϕ is plotted as a function of temperature in Fig. 5(b). The power-law analysis reveals that the temperature-dependent L_ϕ can be perfectly described by $L_\phi \propto T^{-\beta}$, with $\beta = 0.6$. As we know, this scaling exponent is very close to the theoretical expectation $\beta = 1/2$ of 2D electron-electron interaction [16]. Therefore, we can be satisfied that the dominant dephasing mechanism in our $1T$-$TiSe_2$ microflakes is the electron-electron interaction.

IV. CONCLUSION

To summarize, we report the experimental observations of the weak localization effect in the $1T$-$TiSe_2$ microflakes. The nonmonotonic $\rho(T)$ curves revealed the charge-density wave transition at $T_{CDW} \approx 185$ K. And, the low-temperature ($T \lesssim 8$ K) resistivity of $1T$-$TiSe_2$ microflakes is increased with decreasing temperature, and is satisfied with $\rho \propto \ln T$. Furthermore, a MR peak appeared near zero field in the MR curves of $1T$-$TiSe_2$ microflakes, and the low-field MR data can be well described by the Hikami-Larkin-Nagaoka model. The above experimental results demonstrate the weak localization effect in our $1T$-$TiSe_2$ microflakes. The temperature scaling behavior of the phase coherence length predicts the electron-electron interaction plays a dominant role in the electron phase relaxation processes in the $1T$-$TiSe_2$ microflakes at low temperatures.

ACKNOWLEDGMENT

This work is financially supported by the National Natural Science Foundation of China (Grant No. 11604310) and the Key Laboratory of Ultra-Precision Machining Technology Foundation of CAEP (Grant No. ZD18001).

[1] F. J. D. Salvo, D. E. Moncton, and J. V. Waszczak, Phys. Rev. B **14**, 4321 (1976).
[2] J. C. Gill, Contemp. Phys. **27**, 37 (1986).
[3] G. Grüner, Rev. Mod. Phys. **60**, 1129 (1988).
[4] K. C. Woo, F. C. Brown, W. L. McMillan, R. J. Miller, M. J. Schaffman, and M. P. Sears, Phys. Rev. B **14**, 3242 (1976).
[5] T. Rohwer, S. Hellmann, M. Wiesenmayer, C. Sohrt, A. Stange, B. Slomski, A. Carr, Y. Liu, L. M. Avila, M. Kallane, S. Mathias, L. Kipp, K. Rossnagel, and M. Bauer, Nature (London) **471**, 490 (2011).
[6] K. Rossnagel, L. Kipp, and M. Skibowski, Phys. Rev. B **65**, 235101 (2002).
[7] E. Morosan, H. W. Zandbergen, B. S. Dennis, J. W. G. Bos, Y. Onose, T. Klimczuk, A. P. Ramirez, N. P. Ong, and R. J. Cava, Nat. Phys. **2**, 544 (2006).
[8] E. Morosan, K. E. Wagner, L. L. Zhao, Y. Hor, A. J. Williams, J. Tao, Y. Zhu, and R. J. Cava, Phys. Rev. B **81**, 094524 (2010).
[9] A. F. Kusmartseva, B. Sipos, H. Berger, L. Forro, and E. Tutis, Phys. Rev. Lett. **103**, 236401 (2009).
[10] L. J. Li, E. C. T. O'Farrell, K. P. Loh, G. Eda, B. Özyilmaz, and A. H. C. Neto, Nature (London) **529**, 185 (2016).
[11] J. P. Pouget, S. Kagoshima, C. Schlenker, and J. Marcus, J. Phys. Lett. **44**, 113 (1983).
[12] N. P. Ong and P. Monceau, Phys. Rev. B **16**, 3443 (1977).
[13] Q. Cao, F. F. Yun, L. Sang, F. Xiang, G. Liu, and X. Wang, Nanotechnology **28**, 475703 (2017).
[14] J. M. Moya, C.-L. Huang, J. Choe, G. Costin, M. S. Foster, and E. Morosan, Phys. Rev. Materials **3**, 084005 (2019).
[15] M. D. Watson, A. M. Beales, and P. D. C. King, Phys. Rev. B **99**, 195142 (2019).
[16] G. Bergmann, Phys. Rep. **107**, 1 (1984).
[17] B. Hildebrand, C. Didiot, A. M. Novello, G. Monney, A. Scarfato, A. Ubaldini, H. Berger, D. R. Bowler, C. Renner, and P. Aebi, Phys. Rev. Lett. **112**, 197001 (2014).
[18] S. Hikami, A. I. Larkin, and Y. Nagaoka, Prog. Theor. Phys. **63**, 707 (1980).